Examination of evaporative fraction diurnal behaviour using a soil-vegetation model coupled with a mixed-layer model

Jean-Paul Lhomme, E. Elguero

Hydrology and Earth System Sciences, 3(2), *259–270* (1999) © EGS

Hydrology & Earth System Sciences

Examination of evaporative fraction diurnal behaviour using a soil-vegetation model coupled with a mixed-layer model

J.-P. Lhomme[1] and E. Elguero[2]

[1] DICTUS, Universidad de Sonora, AP 1819, Hermosillo, Sonora 83000, Mexico
[2] IMADES, Reyes y Aguascalientes (esq.), Hermosillo, Sonora 83190, Mexico
e-mail for corresponding author: lhomme@cefe.cnrs-mop.fr

Abstract

In many experimental conditions, the evaporative fraction, defined as the ratio between evaporation and available energy, has been found stable during daylight hours. This constancy is investigated over fully covering vegetation by means of a land surface scheme coupled with a mixed-layer model, which accounts for entrainment of overlying air. The evaporation rate follows the Penman-Monteith equation and the surface resistance is given by a Jarvis type parameterization involving solar radiation, saturation deficit and leaf water potential. The diurnal course of the evaporative fraction is examined, together with the influence of environmental factors (soil water availability, solar radiation input, wind velocity, saturation deficit above the well-mixed layer). In conditions of fair weather, the curves representing the diurnal course of the evaporative fraction have a typical concave-up shape. Around midday (solar time) these curves appear as relatively constant, but always lower that the daytime mean value. Evaporative fraction decreases when soil water decreases or when solar energy increases. An increment of saturation deficit above the mixed-layer provokes only a slight increase of evaporative fraction, and wind velocity has almost no effect. The possibility of estimating daytime evaporation from daytime available energy multiplied by the evaporative fraction at a single time of the day is also investigated. It appears that it is possible to obtain fairly good estimates of daytime evaporation by choosing adequately the time of the measurement of the evaporative fraction. The central hours of the day, and preferably about 3 hr before or after noon, are the most appropriate to provide good estimates. The estimation appears also to be much better when soil water availability (or evaporation) is high than when it is low.

Introduction

The evaporative fraction EF is defined as the ratio between evaporation λE and available energy $A (EF = \lambda E/A)$, where A represents the net radiation minus the soil heat flux $(A = R_n - G)$. In many experimental studies over stands of vegetation EF has been found apparently stable during daylight hours. This characteristic of the evaporative fraction makes it potentially interesting for estimating daytime evaporation. If estimates of daytime available energy A_d and instantaneous measurements of EF are available, daytime evaporation λE_d can be simply obtained from $\lambda E_d = EF.A_d$. Daytime available energy A_d is easily estimated from a geostationary satellite or ground based data, and EF can be computed from the satellite at the time of the overpass. This special feature explains why the evaporative fraction has been the subject of many experimental studies, which are briefly reviewed below.

Shuttleworth *et al.* (1989), analysing different sites in the first ISLSCP (International Satellite Land Surface Climatology Project) Field Experiment (FIFE), showed that the midday evaporative fraction was statistically representative of the all-day evaporative fraction. Sugita and Brutsaert (1991) and Brutsaert and Sugita (1992) also analysed FIFE data and confirmed the usefulness of the concept of self-preservation. They concluded that self-preservation tends to produce daytime estimates that are too small by about 5 to 10%, likely caused by the slight upward concavity of the EF curve. Nichols and Cuenca (1993) analysed data from the HAPEX-MOBILHY (Hydrologic Atmospheric Pilot Experiment- Modélisation du Bilan Hydrique) large-scale experiment and found that strong linear relations existed between the midday evaporative fraction and the daylight evaporative fraction. Kustas *et al.* (1993), using data from the MONSOON 90 experiment in Arizona, showed that the correlation coefficient for midday and daytime evaporative fraction was relatively high ($r = 0.92$) under a wide range of conditions. Crago (1996a) extended the work of Nichols and Cuenca

(1993) to FIFE data. He showed that the hypothesis that the midday values of EF are the same as the daytime average values must be rejected at the 0.05 level of significance, confirming however that correlations are high. The same author in another paper (Crago, 1996b) examined the diurnal course of EF and the physics behind the relative partition of available energy. Crago and Brutsaert (1996) compared the self-preservation of EF with that of the Bowen ratio ($\beta = H/\lambda E$, with H the sensible heat flux). They showed that under typical daytime conditions the direct application of the constant evaporative fraction assumption is usually superior to the constant Bowen ratio assumption for the estimation of daytime evaporation, despite the one-to-one correspondence between the two ratios ($\beta = 1/EF - 1$). Stewart (1996) used data taken in Niger to estimate daily evaporation over natural sparse vegetations (savannah and open forest) from the evaporative fraction measured between 09:00 to 10:00 (which corresponds to the overpass of a number of polar orbiting satellites). His conclusion was that this simple extrapolating method is likely to introduce unacceptably large errors in the cases studied. He stressed 'Further research studying the interaction of these variables (those controlling the evaporative fraction), their interaction with each other, and with the development of the convective boundary layer, will be necessary to define the conditions when the evaporative fraction can be treated as conservative' (Stewart, 1996, p. 253).

Most of the studies concerning the self-preservation of the evaporative fraction and its interest in estimating daytime evaporation have been purely experimental. The results obtained are a little ambiguous and not totally convincing. In the following study a different approach is used, based upon the idea of Stewart (1996) quoted above. Our purpose is to use the modelling approach to examine the diurnal behaviour of the evaporative fraction, since the entire diurnal course of air and surface characteristics can be adequately simulated. A model allows one to simulate a much larger variety of experimental conditions than experiments can generally provide. More specifically, the aim of this paper is to perform simulations of the Convective Boundary Layer (CBL) development over vegetated surface and to examine the corresponding behaviour of the evaporative fraction. The development of the CBL is a phenomenon that occurs during daylight hours in most fair-weather conditions, when a layer of strong convective turbulence progressively grows, incorporating surface fluxes (sensible heat, water vapour) and overlying air into itself. At night the fluxes are relatively small in magnitude, and the evaporative fraction is highly unstable and sometimes undefined (Nichols and Cuenca, 1993). For this reason, it is justified to restrict the analysis to the daylight period. The coupling of a growing convective boundary layer with a surface parameterisation has already been employed to investigate the constancy of the Priestley-Taylor coefficient α (De Bruin, 1983; Culf, 1994; Lhomme, 1997; Huntingford and Monteith, 1998), but in a perspective different from the one used here. The coefficient α is related to the evaporative fraction by $EF = [\varepsilon/(\varepsilon+1)]\alpha$, where ε is the dimensionless slope of the saturation specific humidity. Both coefficients (EF and α) have been analysed by Betts (1994) in the light of a mixed-layer model: he stressed that over moist land surfaces EF lies between two reference values during the peak of the daytime heating cycle. Raupach (1998) has studied with many details the local feedbacks occuring on land-air exchanges and has shown how boundary-layer feedbacks can modulate evaporative fluxes. This paper follows the lines drawn by these authors. The first section details the characteristics of the model used to simulate the diurnal pattern of the evaporative fraction: a soil-vegetation model coupled with a mixed-layer model accounting for entrainment. In the second section, the numerical results obtained in different scenarios are analysed, placing emphasis on the self-preservation of the evaporative fraction.

Model description

THE SOIL-VEGETATION MODEL

The Penman-Monteith single-source model (Monteith, 1981) is used to calculate the flux of transpiration. It is written in the form of the following equation

$$\lambda E = \frac{\varepsilon(R_n - G) + \rho\lambda D / r_a}{\varepsilon + 1 + r_s / r_a} \qquad (1)$$

$D = q^*(\theta) - q$ is the potential saturation deficit of the air (with θ the air temperature and q the specific humidity of the air); ε (specified above) varies with air temperature; ρ is the air density; λ is the latent heat of vaporisation; r_a is the bulk aerodynamic resistance to heat and water vapour transfer through the surface layer and r_s is the bulk surface resistance to water vapour transfer. G is the soil heat flux and R_n is the net radiation given by $R_n = (1 - a)S + \varepsilon_v(L - \sigma T_s^4)$, where S is the incoming solar radiation (input to the model), L is the incoming long-wave radiation, a is the vegetation albedo, ε_v is the vegetation emissivity, σ is the Stefan-Boltzmann constant and T_s is the surface temperature inferred from the energy balance equation. Soil heat flux G is calculated as a given fraction of R_n ($G = f.R_n$) and L is obtained from the following equation (Brutsaert, 1982): $L = \varepsilon_a\sigma\theta^4$ with $\varepsilon_a = 0.552e^{1/7}$, where θ is the air temperature in Kelvin and e is the vapour pressure in the well mixed layer expressed in hPa. Aerodynamic resistance r_a is calculated following the formulation proposed by Choudhury *et al.* (1986), which takes into consideration the stability corrections. It is given by

$$r_a = r_{a,0} / (1 + \eta)^p \quad \text{with} \quad r_{a,0} = \ln^2(z_r / z_0) / (k^2 U) \qquad (2)$$

where z_0 is the roughness length, $k = 0.4$ is the van Karman constant, U is the wind velocity at a reference

height z_r. The parameter p is equal to 3/4 in unstable conditions and η is given by $\eta = 5z_r g(T_s - T)/(TU^2)$, where $g = 9.81$ m s^{-2} is the acceleration of gravity, T_s is the surface temperature and T is the air temperature in Kelvin at the reference height z_r (T is assumed to be equal to the potential temperature of the well mixed layer θ). The evaporative fraction can be put in the following form (inferred from Eqn. (1))

$$EF = \lambda E/(R_n - G) = (1+X)/(1+Y) \qquad (3)$$

with

$$X = \rho\lambda[D/(R_n - G)]/(\varepsilon r_a) \quad \text{and} \quad Y = (1 + r_s/r_a)/\varepsilon \qquad (4)$$

D is obtained from the mixed-layer model (see below) and the surface resistance (r_s) is calculated as follows.

The bulk surface resistance to water vapour transfer r_s is parameterised according to a Jarvis type model (Jarvis, 1976). So far, these models have represented the most common way of parameterizing the response of stomata to environmental factors, at leaf scale as well as at canopy scale (Stewart, 1988). They describe this response in the form of a minimal resistance multiplied by the product of independent stress functions interacting without synergy

$$r_s = r_{s\,\min} F_1(S) F_2(T) F_3(D) F_4(\Psi_l) \qquad (5)$$

Here, r_{smin} is the minimum stomatal resistance observed in optimal conditions, i.e. if none of the controlling variables is limiting. Kelliher *et al.* (1995) showed that r_{smin} takes average values of 30 and 50 s m^{-1} respectively for agricultural crops and natural vegetation. S is the incoming solar radiation, T is the air temperature, D is the water vapour saturation deficit, Ψ_l is the leaf water potential. The influence of CO_2 is generally omitted because its concentration is almost constant during the diurnal part of the day. Each function (F_i) varies from unity to infinity. The influence of solar radiation can be expressed as a hyperbolic function of the form (Stewart, 1988)

$$F_1(S) = (c + S)/(dS) \qquad (6)$$

where d is obtained from $d = 1 + c/1000$. When S is expressed in W m^{-2}, Stewart (1988) derived a mean value of about 100 for c in the case of a pine forest in England, and Stewart and Gay (1989) a mean value of about 400 in the case of the Konsa Prairie in Kansas (FIFE data). In many parameterisations of stomatal resistance the effect of temperature is neglected (Stewart and Gay, 1989; Lynn and Carlson, 1990; Mascart *et al.*, 1991; de Ridder and Schayes, 1997). In our analysis, for the sake of convenience, we also assume that ambient temperature has no effect on stomatal resistance and thus $F_2(T) = 1$. As regards the dependence on saturation deficit $F_3(D)$, the common form generally adopted is a linear decrease of stomatal conductance with D (Jarvis, 1976; Stewart, 1988; Noilhan and Planton, 1989) leading to

$$F_3(D) = (1 - \alpha D)^{-1} \quad \text{and} \quad 0 < D < 1/\alpha \qquad (7)$$

For the Konza Prairie in Kansas (FIFE data), Stewart and Gay (1989) give a mean value of about 24 to the empirical coefficient α, with D expressed in kg kg^{-1}. In Noilhan and Planton (1989), the value of α (derived for a coniferous forest from the HAPEX-MOBILHY data set) is equal to 41. Several stomatal models do not take into account the effect of saturation deficit (Deardorff, 1978; Mascart *et al.*, 1991; de Ridder and Schayes, 1997). The dependence of stomatal resistance on leaf water potential can be expressed in different ways. Choudhury and Idso (1985) derived the following empirical function from data obtained on field-grown wheat

$$F_4(\Psi_l) = 1 + (\Psi_l/\Psi_c)^n \quad \text{with} \quad n = 5.5 \qquad (8)$$

where Ψ_l is the bulk leaf water potential and Ψ_c is a critical leaf water potential giving the limit beyond which the transpiration rate is strongly limited by water stress (about −2 MPa for a cereal crop). The bulk leaf water potential is not known *a priori*, but it is coupled to soil water status and surface resistance can be calculated in the way described in the Appendix. The main reasons for variation in surface resistance are solar radiation and leaf water potential. The effect of saturation deficit is relatively weak, compared to the effects of solar radiation and leaf water potential, and can be interpreted as an indirect action through transpiration and leaf water potential (Lhomme *et al.*, 1998). In this very reference it is also shown that a relation between surface resistance and transpiration, similar to the relation proposed by Monteith (1995), can be obtained by transforming the function involving leaf water potential with the help of van den Honert's equation (see Appendix).

THE MIXED-LAYER MODEL

The mixed-layer model used represents an adaptation of the slab-model originally devised by McNaughton and Spriggs (1986), where the CBL is seen as a well-mixed layer with a potential temperature, θ, and a specific humidity, q, constant with height, topped by the undisturbed atmosphere, whose properties are determined by synoptic scale processes. Between the ground surface and the well-mixed layer there is a relatively thin surface layer of height z_r, where the gradients of temperature and humidity may be significant. The inversion cap of the CBL, whose height, h, grows during the daytime, is not impermeable. The incorporation of a thin layer of air of thickness, dh, potential temperature, $\theta_+(h)$, and humidity, $q_+(h)$, into the mixed-layer with potential temperature, θ, and specific humidity, q, leads to the following differential equations, respectively for sensible heat and water vapour (McNaughton, 1989)

$$\rho c_p h \frac{d\theta}{dt} = H + \rho c_p(\theta_+ - \theta)\frac{dh}{dt} \qquad (9)$$

$$\rho h \frac{dq}{dt} = E + \rho(q_+ - q)\frac{dh}{dt} \quad (10)$$

where H is the sensible heat flux (obtained from the energy balance equation $H = A - \lambda E$) and E is the evaporation flux at the surface given by Eqn. (1) (in which D is the potential saturation deficit within the mixed layer). Generally $\theta_+(h) > \theta$ and $q_+(h) < q$, which means that entrainment tends to raise the temperature and to decrease the humidity within the CBL, both factors contributing to increase the evaporation rate. The rate of growth of the CBL is parameterized according to the relationship proposed by McNaughton and Spriggs (1986)

$$\frac{dh}{dt} = \frac{H}{\rho c_p h \gamma_\theta} \quad (11)$$

where γ_θ is the gradient of potential temperature just above the inversion base and H is assumed to be positive. This closure equation is not physically based, but it gives similar results to more complex formulae (Culf, 1992). Eqns. (9), (10) and (11) have three dependent variables ($\theta(t)$, $q(t)$, $h(t)$) and form a set of three coupled first-order differential equations, which are solved using the Runge-Kutta numerical method. The calculation is initiated with a fixed value of the CBL height h_0. The parameters ρ, γ, c_p and γ_θ are taken as constant and ε varies with the potential temperature θ of the mixed-layer. It is worthwhile stressing that the above modelling is valid only for uniform vegetation surfaces extensive enough for the CBL to reach full equilibrium with the underlying surface.

The vertical profiles of potential temperature and specific humidity in the undisturbed atmosphere are taken as linear

$$\theta_+(z) = \gamma_\theta . z + \theta_{+0} \quad \text{and} \quad q_+(z) = \gamma_q . z + q_{+0} \quad (12)$$

where γ_q is the gradient of specific humidity just above the CBL, θ_{+0} and q_{+0} are the potential temperature and the specific humidity above the CBL extrapolated at $z = 0$. The standard profiles used in the simulations are the so-called McClatchey profiles as cited by Jacobs (1994). They represent average atmospheric conditions in terms of latitude and season. One case has been considered here, the Mid Latitude Summer (MLS) case, and linear equations have been fitted to the curves given by Jacobs (1994, p. 156): $\theta_+ = 4.78\ z + 293.6$ and $q_+ = -0.00285\ z + 0.01166$, with z expressed in km, θ in K and q in kg kg^{-1}. The initial values of potential temperature θ_0 and specific humidity q_0 are taken to be equal respectively to $\theta_+(h_0)$ and $q_+(h_0)$.

Solar radiation $S(t)$ is assumed to vary as a sine wave, which intends to simulate its diurnal behaviour over the day length δ: $S(t) = 0$ at the initial time $t = t_0$ (sunrise) and at the time $t = t_0 + \delta$, (sunset). $S(t) = S_x$ (a maximum value) at the time $t = t_0 + \delta/2$ which coincides with midday. Under these conditions $S(t)$ can be written as

$$S(t) = S_x \sin[\pi(t - t_0)/\delta] \quad (13)$$

In the simulations performed, $\delta = 14$ h and $t_0 = 5$ h (solar time). The model runs from t_0 to $t_0 + \delta$, but the coupling with the CBL occurs only when the surface temperature T_s is greater than the potential temperature within the mixed layer θ (i.e., when $H > 0$).

There would be a simple way of modelling a passage of clouds, at least in theory. One can assume it reduces the incoming solar radiation S_x in a constant ratio during a certain period of time beginning at a given time. It should be emphasised, however, that a contradiction exists to some extent between this simple approach and the CBL modelling. The CBL develops in most fair-weather conditions, but not when the atmosphere is disturbed by fronts, by deep cumulus convection or by storms (Raupach *et al.*, 1992). Precisely, it is in this very case that passages of clouds generally occur. Furthermore, since short cloudy spells have an effect only on a small patch, they cannot be accounted for by the mixed-layer model (the modelling approach assuming the cloudy spells to affect the whole surface in equilibrium with the CBL). Another reason against the simulation of passage of clouds is linked to thermal and stomatal inertia. In our approach, soil-canopy thermal inertia is not taken into account and stomatal resistance is assumed to react immediately to any change in solar radiation input. In the case of short passages of clouds generating a succession of transient states, the thermal inertia and the response time of stomata could play an important role. For all the reasons mentioned above, scenarios involving cloudy spells have been disregarded.

Numerical results and discussion

PERFORMANCE OF THE MODEL

The mixed-layer model presented has been tested by McNaughton and Spriggs (1986) with experimental data from Cabauw in the Netherlands. It has also been used by the same authors to evaluate the Priestley-Taylor equation and the complementary relationship (McNaughton and Spriggs, 1989). In the original model, the coupling between the surface and the atmosphere is obtained only through the saturation deficit of the air D which drives Eqn. (1), the bulk surface resistance r_s being maintained constant throughout the day. In the present study, the original model has been upgraded by adding a second coupling between the surface and the atmosphere, which acts through the surface resistance. The parameterisation used for this resistance has been tested successfully against FIFE data in conditions of small soil moisture deficits (Stewart and Gay, 1989): It involves solar radiation (Eqn. (6)), saturation deficit (Eqn. (7)) and transpiration rate (Eqn. (A4)) through leaf water potential (Ψ_l). In the mixed-layer model recently used by Kim and Entekhabi (1997) to examine the Priestley-Taylor equation and the

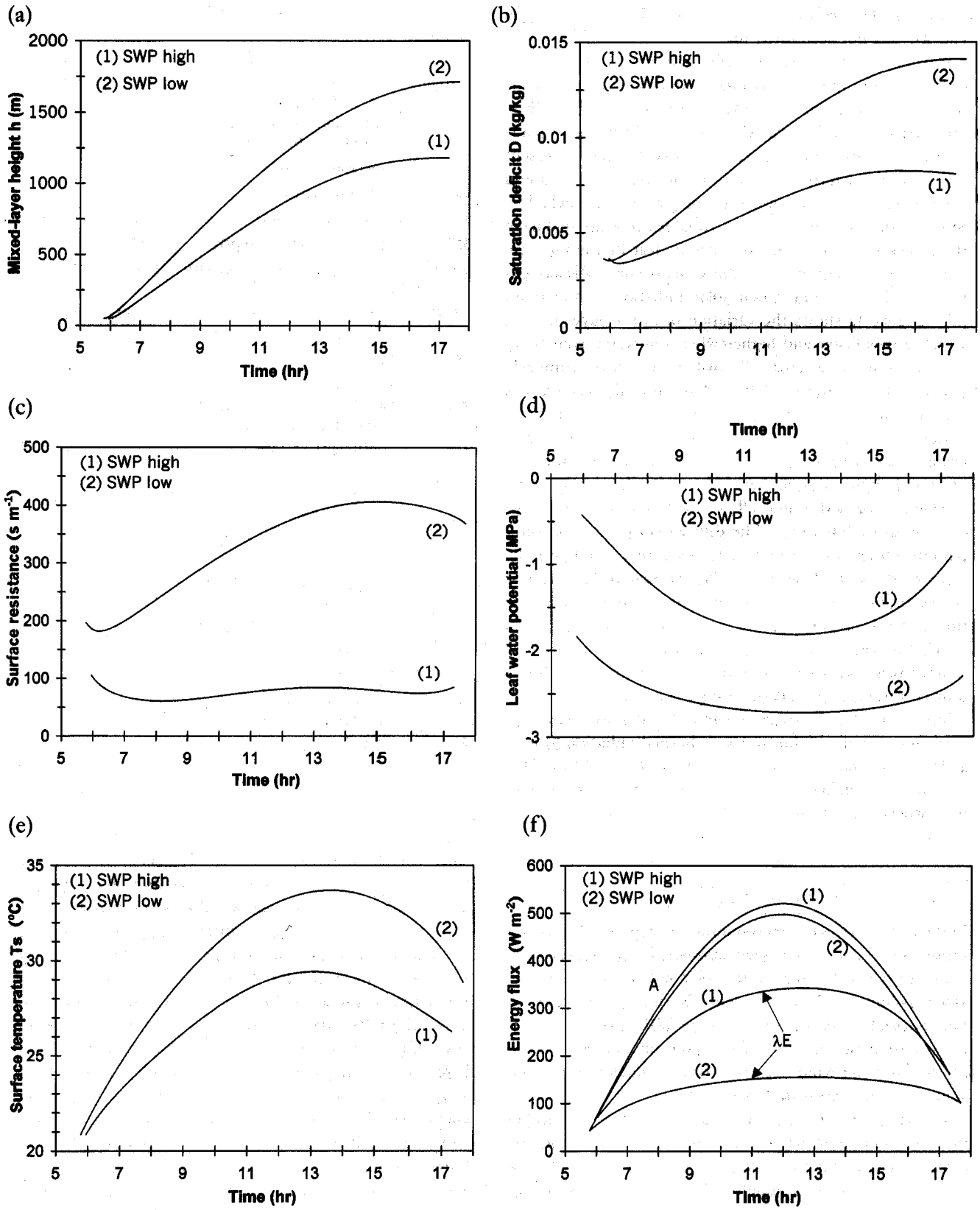

Fig. 1. *Diurnal variation of several magnitudes for two different values of soil water potential (SWP): (1) Ψ_s= –0.1 MPa, (2) Ψ_s = –1.5 MPa, with S_x = 800 W m^{-2}, U = 4 m s^{-1} and Mid Latitude Summer profiles above the mixed-layer: (a) mixed-layer height h; (b) saturation deficit within the mixed-layer D; (c) surface resistance r_s; (d) leaf water potential Ψ_l; (e) surface temperature T_s; (f) available energy A and evaporation λE.*

complementary relationship, the dependence of r_s on Ψ_l and λE was not accounted for.

Several figures (Figs. 1a to 1f) are presented to show the outputs of the model in standard conditions for two contrasted values of soil water availability: a high value (Ψ_s = –0.1 MPa) and a low value (Ψ_s = –1.5 MPa). The parameters kept constant are listed in Table 1. They represent the main characteristics of the soil and the vegetation and some basic data concerning the mixed-layer model. The diurnal course of the relevant variables is plotted during the period of time when the sensible heat flux is positive, i.e. when the coupling with the CBL occurs. Midday coincides with the time when solar radiation is maximum (S_x). Figure 1a shows the variation of mixed-layer height, which grows faster and higher when soil water availability is weak due to a greater sensible heat flux. Similarly (Fig.1b), the saturation deficit of the mixed layer reaches a greater value when soil water potential is low. In Fig. 1c, surface resistance is plotted versus time. When soil water availability is high (Ψ_s = –0.1 MPa), r_s remains almost constant and slightly lower than 100 s m^{-1}, whereas for a low availability of soil water (Ψ_s = –1.5 MPa), r_s increases rapidly up to 400 s m^{-1}. The diurnal course of leaf water potential Ψ_l is plotted in Fig. 1d: evidently, the lower the soil water potential the lower Ψ_l . Surface temperature is shown in Fig. 1e. For a low soil water potential, evaporation is weak and T_s reaches a maximum value of about 34°C, whereas for a high potential, the maximum surface temperature obtained is around 29°C. Figure 1f gives the diurnal variation of available energy A and evaporation λE. Available energy is lower when soil water availability is weak because of a higher upward thermal radiation (due to a higher surface temperature). For Ψ_s = –0.1 MPa, evaporation reaches a maximum value of around 350 W m^{-2}, whereas for Ψ_s = –1.5 MPa, λE does not exceed 150 W m^{-2}.

Table 1. Values of the variables kept constant in the simulations.

Variable	Significance	Value and unit
f	Dimensionless coefficient for soil heat flux calculation	0.05
a	vegetation albedo	0.20
ε_v	vegetation emissivity	0.97
r_{rs}	root-stem resistance	0.005 MPa (W m^{-2})$^{-1}$
Z_{ef}	effective rooting depth	1 m
K_{sat}	soil hydraulic conductivity at saturation	6.3×10^{-6} m s^{-1}
Ψ_{sat}	soil water potential at saturation	–0.003 MPa
B	Coefficient in the relation $K_s = f(\Psi_s)$	7.1
r_{smin}	minimum canopy stomatal resistance	40 s m^{-1}
C	coefficient in the stress function $F_1(S)$	400
α	coefficient in the stress function $F_3(D)$	24
Ψ_c	critical leaf water potential in $F_4(\Psi_l)$	–2.0 MPa
z_0	roughness length of the vegetation canopy	0.05 m
z_r	reference height for wind velocity	50 m
δ	day length	14 h
t_0	initial time for the simulation process	5 h
h_0	CBL height at $t = t_0$	50 m

DIURNAL BEHAVIOUR OF THE EVAPORATIVE FRACTION

Different scenarios corresponding to different values of input parameters have been simulated. The parameters which vary are the maximum solar radiation S_x, the soil water potential Ψ_s (which controls the canopy stomatal resistance), the conditions above the CBL (more precisely, the profile of specific humidity in the undisturbed atmosphere), and the wind velocity. The parameters kept constant are those listed in Table 1.

Figures 2 to 4 show the diurnal evolution of the evaporative fraction for different conditions of solar radiation, soil water potential and humidity profile above the CBL. These simulated results have roughly the same behaviour as the experimental results shown, for instance, by Brutsaert and Sugita (1992) from FIFE data: The diurnal course of EF presents always a typical upward concavity. In Figure 2, the evaporative fraction is plotted as a function of time for three different values of maximum solar radiation S_x (600, 800 and 1000 W m^{-2}). The evaporative fraction decreases when solar energy increases, but it always conserves the same upward concavity. Figure 3 shows the diurnal evolution of EF for three different values of soil water potential Ψ_s (–0.1, –1.0, –1.5 MPa). As could be anticipated, EF decreases with Ψ_s. It passes from a minimum of 0.65 for Ψ_s = –0.1 MPa to a minimum of 0.3 for Ψ_s = –1.5 MPa. Figure 4 shows the diurnal course of EF for three different conditions above the CBL adapted from the Mid Latitude Summer case. The vertical profile of potential temperature has been kept constant, and in the profile of specific humidity ($q_+(z) = \gamma_q z + q_{+0}$), only the value of q_{+0} (the specific humidity above the CBL extrapolated at z = 0) has been varied of –25% and –50%. This variation corresponds in fact to a horizontal translation of the humidity profile in a set of axes: $x = q$ and $y = z$. It appears that changing the conditions above the CBL has only a slight impact on the evaporative fraction diurnal course, this impact being more sensible in the early hours of the day. As regards wind velocity, it has almost no impact on the course of the evaporative fraction (the corresponding figure is not presented because

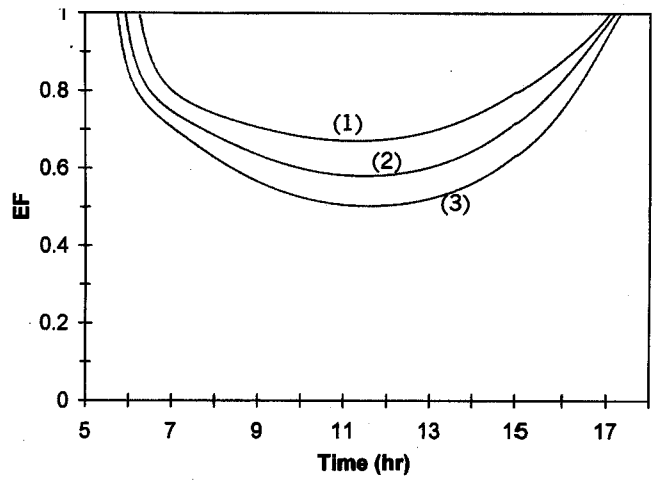

Fig. 2. *Diurnal course of evaporative fraction EF for three different values of maximum solar radiation S_x : (1) 600 W m^{-2}, (2) 800 W m^{-2}, (3) 1000 W m^{-2}, with Ψ_s= –0.5 MPa, U = 4 m s^{-1} and Mid Latitude Summer conditions above the mixed-layer.*

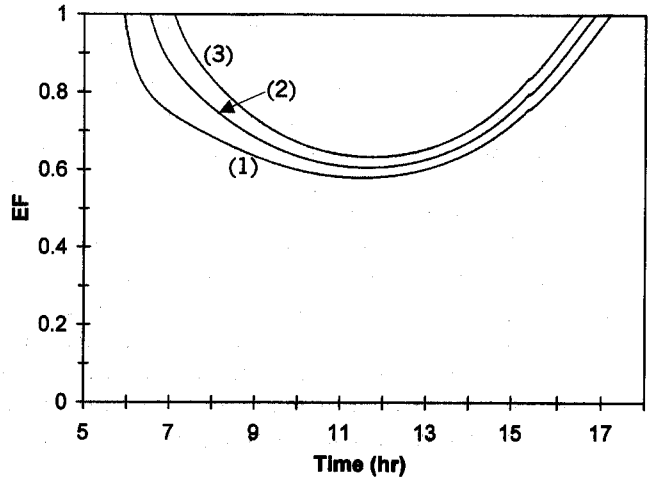

Fig. 4. *Diurnal course of evaporative fraction EF for three different conditions above the mixed-layer adapted from the Mid Latitude Summer case: (1) q_{+0} = 0.0117 kg kg^{-1}, (2) q_{+0} = 0.0088 (–25%), (3) q_{+0} = 0.0058 (–50%), with S_x = 800 W m^{-2}, Ψ_s = –0.5 MPa and U = 4 m s^{-1}.*

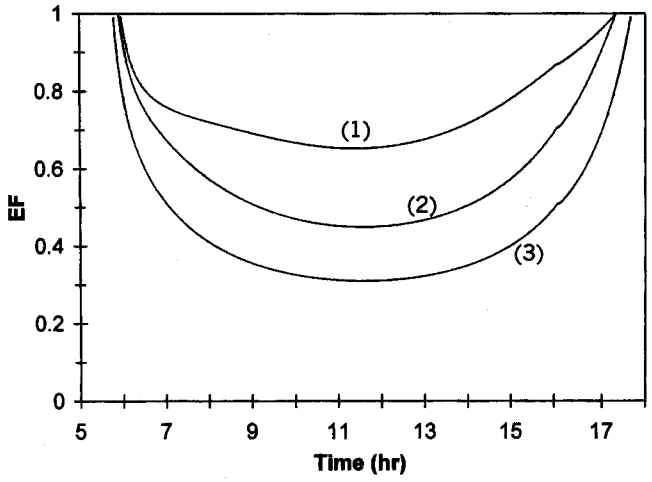

Fig. 3. *Diurnal course of evaporative fraction EF for three different values of soil water potential Ψ_s : (1) –0.1 MPa, (2) –1.0 MPa, (3) –1.5 MPa, with S_x = 800 W m^{-2}, U = 4 m s^{-1} and Mid Latitude Summer conditions.*

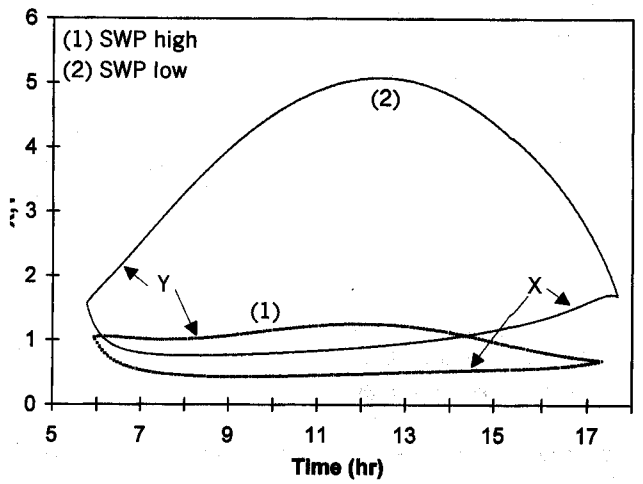

Fig. 5. *Diurnal course of X and Y (Eqn. (4)) for two different values of soil water potential Ψ_s : (1) –0.1 MPa, (2) –1.5 MPa, with S_x = 800 W m^{-2}, U = 4 m s^{-1} and Mid Latitude Summer conditions.*

the curves drawn for different values of wind velocity cannot be distinguished). From the graphs drawn above two major points can be deduced: (i) the diurnal course of the evaporative fraction presents an upward concavity and is relatively constant in the central hours of the day; (ii) the evaporative fraction around the midday hours is always lower than the daytime mean value because of the particular shape of the diurnal curve. It is important to stress that these results hold only in conditions of fair weather (without cloudy spells).

In order to understand better the diurnal behaviour of *EF* and the sources of variation, the parameters *X* and *Y* of Eqns. (3) and (4) have been plotted in Fig. 5 as a function of time for two scenarios: one without water stress (Ψ_s = –0.1 MPa), the other with water stress (Ψ_s= –1.5 MPa). It appears that during the central hours of the day *X* is relatively constant and does not vary a lot from one scenario to another, whereas *Y* can be much more variable in the central hours and from one scenario to another. This means that the parameters *D*, *A* and r_a in *X* have a kind of compensating effect which cancels their respective variation. The main variation in *EF* comes from *Y*, i.e., the ratio r_s/r_a.

EFFECTS OF ENVIRONMENTAL CONDITIONS ON THE EVAPORATIVE FRACTION

Simulations have been carried out to assess the variation of the evaporative fraction as a function of environmental conditions. For each scenario simulated by the model, the

mean value of the evaporative fraction during the daytime EF_d and the midday evaporative fraction EF_m have been determined. EF_m is calculated as the ratio between the midday evaporation and the midday available energy and EF_d as the ratio between the mean evaporation (λE_d) and the mean available energy (A_d) during the daytime. The daytime, d, is taken as the period when the sensible heat flux is positive ($H > 0$), i.e. when the coupling between the surface and the mixed-layer occurs. It corresponds approximately to the time of day when $A = R_n - G > 0$. The duration of d depends upon the amount of solar radiation, but it is always shorter than the day length δ, defined as the duration between sunrise and sunset. However, most of the evaporation process occurs during d.

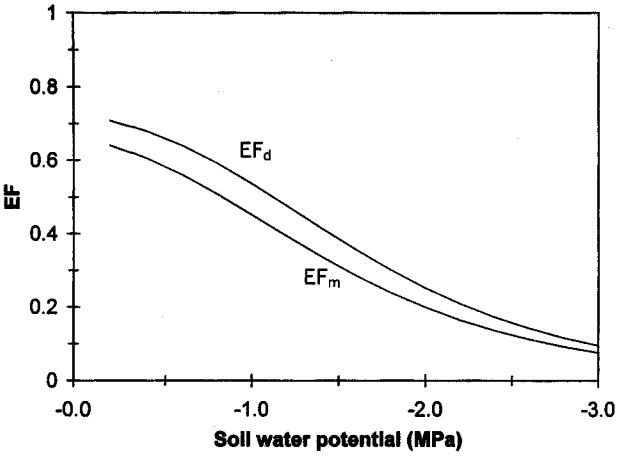

Fig. 6. *Daytime and midday evaporative fractions (EF_d and EF_m) versus soil water potential with S_x = 800 W m^{-2}, U = 4 m s^{-1} and Mid Latitude Summer conditions.*

In Fig. 6, daytime and midday evaporative fractions (EF_d and EF_m) are plotted versus soil water potential. Both curves have a sigmoid shape, the evaporative fraction decreasing when Ψ_s decreases. EF_d diminishes from about 0.7 (for a potential close to 0) to 0.1 (for a potential close to –3 MPa). As could be anticipated, the evaporative fraction is a strongly increasing function of soil water availability. A similar variation, slightly shifted, occurs for EF_m. The midday evaporative fraction EF_m is always lower than daytime evaporative fraction EF_d because of the upward concavity of the curves representing the diurnal course of EF. In Fig. 7, the evaporative fraction is plotted against maximum solar radiation S_x which varies from 500 W m^{-2} to 1000 W m^{-2} (low values of S_x have not been considered because they lead to very short daytime periods (d), defined as the period when $H > 0$). EF_d and EF_m decrease when S_x increases, but their respective decreases do not exceed 0.2, which is relatively weak. Similar results have been shown in Huntingford and Monteith (1998). In Fig. 8, the evaporative fraction is plotted against wind velocity U at 50 m, which varies from 1 m s^{-1} to 10 m s^{-1}. As almost no variation occurs, the evaporative fraction

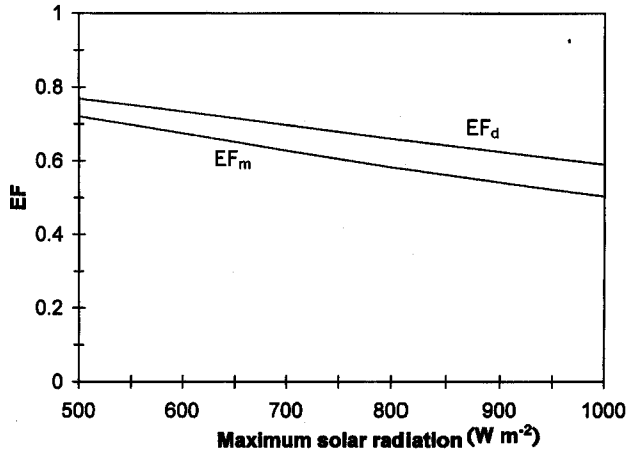

Fig. 7. *Daytime and midday evaporative fraction (EF_d and EF_m) versus maximum solar radiation S_x with Ψ_s = –0.5 MPa, U = 4 m s^{-1} and Mid Latitude Summer conditions.*

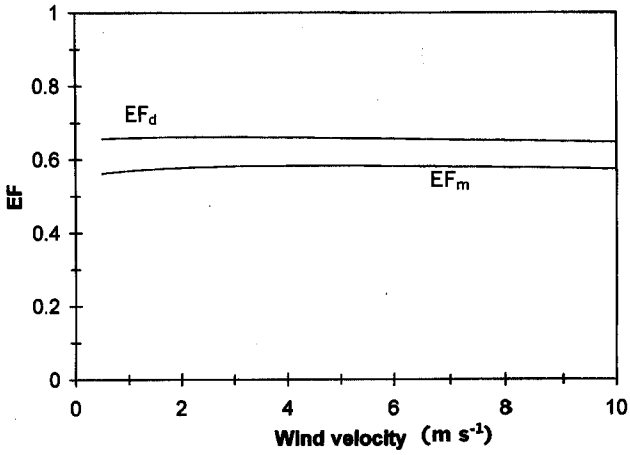

Fig. 8. *Daytime and midday evaporative fraction (EF_d and EF_m) versus wind velocity (at a reference height of 50 m) with S_x = 800 W m^{-2}, Ψ_s = –0.5 MPa and Mid Latitude Summer conditions.*

appears to be insensitive to wind velocity variation. The saturation deficit above the CBL ($D_+ = q^*(\theta_+) - q_+$) is an important factor which influences the conditions within the mixed-layer through the air incorporated by the entrainment effect. To assess its influence the following simulations have been performed with the Mid Latitude Summer case. As for Fig. 4, the vertical profile of potential temperature has been kept constant, and in the profile of specific humidity, only the value of q_{+0} (the specific humidity above the CBL extrapolated at z = 0) has been changed. The corresponding D_{+0} (saturation deficit above the CBL extrapolated at z=0) has been varied from 0 to 0.010 kg kg^{-1}, which means that q_{+0} varies from $q^*(\theta_{+0}) = q^*(293.6)$ = 0.015 to 0.005 kg kg^{-1}. In Fig. 9, the evaporative fraction is plotted against D_{+0}. It appears that both EF_d and EF_m increase with D_{+0}, but their respective variation is rather weak (less than 0.1).

ESTIMATION OF DAYTIME EVAPORATION FROM INSTANTANEOUS MEASUREMENTS OF *EF*

One of the main interests of the pseudo-constancy of the evaporative fraction during daylight hours lies in the possibility of estimating daytime evaporation from instantaneous measurements of *EF* and estimates of daytime available energy. To test this pseudo-constancy, the daytime evaporation λE_d (as obtained from the model) has been compared to the estimate $\lambda E_{d,e}$ calculated from $\lambda E_{d,e} = EF_i.A_d$, where EF_i is the evaporative fraction measured at one time of the day and A_d is the daytime available energy. Daytime is always taken as the period (d) when the sensible heat flux is pointed upwards. Four scenarios have been simulated and for each the different times of the day have been tested. Solar radiation and soil water potential being the variables with the strongest effect on the evaporative fraction, each scenario corresponds to a different combination of two values of S_x (high and low) and two values of Ψ_s (high and low). Wind velocity and air humidity above the CBL, which have a very weak impact, have been disregarded. The different scenarios (A, B, C, D) are specified in Table 2.

Figures 10a and 10b show the results obtained for each scenario. In these figures, the straight line represents the daytime evaporation λE_d calculated from the model, and the curved line represents the estimates $\lambda E_{d,e}$ obtained from the evaporative fraction at the corresponding time.

Table 2. Scenarios simulated to estimate daytime evaporation from a point measurement of *EF*.

Scenario	A	B	C	D
S_x (W m^{-2})	1000	1000	600	600
Ψ_s (MPa)	–0.1	–1.5	–0.1	–1.5

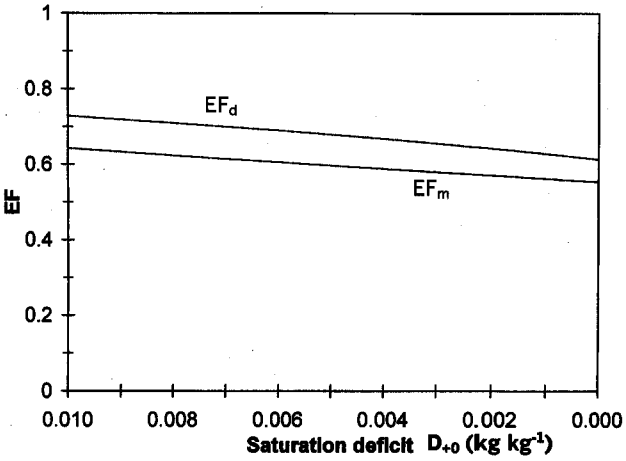

Fig. 9. *Daytime and midday evaporative fraction (EF_d and EF_m) versus saturation deficit above the CBL extrapolated to z = 0 (D_{+0}). S_x = 800 W m^{-2}, Ψ_s = –0.5 MPa and U=4 m s^{-1}.*

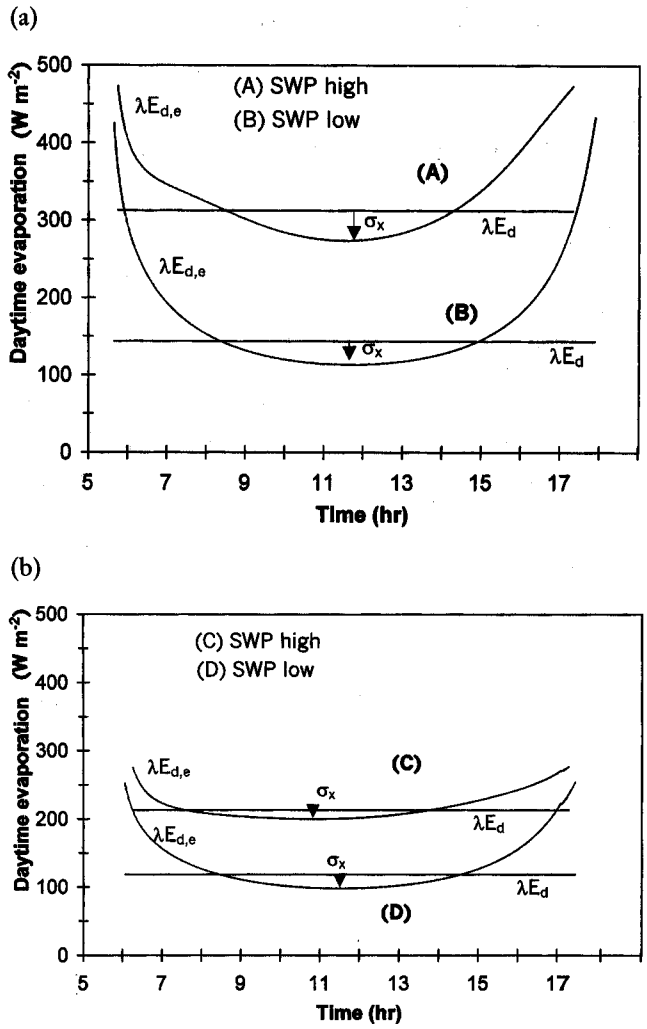

Fig. 10. *Diurnal evolution of $\lambda E_{d,e}$ (daytime evaporation estimated from the evaporative fraction at the corresponding time) compared with the real daytime evaporation λE_d simulated by the model for the 4 scenarios presented in Table 2: (a) scenarios A and B (S_x = 1000 W m^{-2}); (b) scenarios C and D (S_x = 600 W m^{-2}). SWP = soil water potential.*

The two curves intersect around 08:00–09:00 in the morning and 14:00–15:00 in the afternoon. These intercepts, which correspond to perfect estimates, are apparently not symmetrical with respect to noon (the time interval between the first intercept and noon is larger than the one between noon and the second intercept). Using the evaporative fraction at one time in the central hours (defined as the ones between the two intercepts) leads to a systematic underestimation of the daytime evaporation (evidently because of the particular upward concavity of the *EF* curves). Conversely, the early and late hours of the day lead to a systematic overestimation. Whereas the estimates obtained from the central hours never depart very strongly from the reference value, those obtained early in the morning or late in the afternoon can be very different. This means practically that it is recommended to use the

evaporative fraction of the central hours (and preferably those measured 3–4 hr before or 2–3 hr after midday) for obtaining good estimates of daytime evaporation. For the four scenarios (A, B, C, D) simulated, we have calculated the maximum error (σ_x) made on the estimation of daytime evaporation from a single measurement of EF during the central hours of the day (i.e. between the two intersection points). These errors are visualised on the corresponding figures and their values are reported in Table 3, together with the relative error ($re_x = \sigma_x / \lambda E_d$) made on the estimation of daytime evaporation. The results indicate that (i) the estimation can be made with an error lower than 10% if the single measurement is correctly chosen during the central hours of the day, (ii) the estimation is much better when soil water availability is high than when it is low, (iii) for a same soil water potential, the accuracy of the estimation increases when solar radiation decreases.

Table 3. Maximum error $\sigma_x = max(\lambda E_d - \lambda E_{d,e})$ and corresponding relative error ($re_x = \sigma_x / \lambda E_d$) on the estimation of daytime evaporation from a single measurement of EF in the central hours of the day for the different scenarios of Table 2.

Scenario	A	B	C	D
λE_d (W m^{-2})	313	143	213	118
σ_x (W m^{-2})	–39	–30	–13	–20
re_x (%)	–12	–21	–6	–17

The influence of vegetation characteristics on the accuracy of the estimation of daytime evaporation has also been investigated by varying the roughness length z_0 (Eqn. (2)) and the minimum stomatal resistance r_{smin} of the vegetation (Eqn. (5)). For the following standard conditions (S_x = 800 W m^{-2}, Ψ_s = –0.1 MPa, U = 4 m s^{-1} and Mid Latitude Summer case), all other conditions being equal, the maximum relative error (re_x) on daytime evaporation during the central hours of the day, calculated as above, is –8% and –10% respectively for z_0 = 0.01 m (grass) and z_0 = 1.0 m (forest). For the same standard conditions and z_0 = 0.05 m, the value of re_x is –8% and –12% respectively for r_{smin} = 20 s m^{-1} and r_{smin}=200 s m^{-1}. These results tend to prove that the accuracy of the estimation of daytime evaporation from the central hours of the day is slightly better for low roughness and low minimum stomatal resistance, all else being equal.

Conclusion

The evaporative fraction, which has been found experimentally stable during daylight hours, has been investigated by means of a mixed-layer model coupled with a soil-vegetation model. The land-surface scheme is based upon the Penman-Monteith equation. Canopy stomatal resistance is parameterized according to a Jarvis type formulation involving three different controlling variables (solar radiation, water vapour saturation deficit, leaf water potential), this last control being linked to soil water status through van den Honert's equation. In conditions of fair weather and over fully-covering vegetation the following conclusions can be drawn from the simulated scenarios.

The curve representing the diurnal course of the evaporative fraction has a typical concave-up shape and is relatively constant around midday. Because of this particular shape, the evaporative fraction in the central hours of the day is always lower that the daytime mean value. The evaporative fraction decreases when soil water decreases or when solar energy increases. It increases slightly with the saturation deficit above the CBL. Wind velocity has no effect on it. The daytime evaporation λE_d, as calculated from the model, has been compared to the estimate $\lambda E_{d,e}$ obtained by multiplying the daytime available energy by the evaporative fraction measured at one time of a day. It appears that by choosing adequately the time of the measurement of the evaporative fraction it is possible to obtain fairly good estimates of λE_d (less than 10%). For that it is recommended to use the evaporative fraction of the central hours and preferably those measured about 3 hr before or after noon (solar time). The estimates obtained in this way appear to be much better when soil water availability (or evaporation) is high than when it is low.

It is worth stressing, however, that these conclusions hold only in conditions of fair weather and that the presence of cloudy spells may contradict these results.

Appendix: Coupling the surface resistance with soil water status

The bulk leaf water potential Ψ_l appearing in Eqn. (8) is related to the bulk soil water potential Ψ_s (which measures the soil water availability for the vegetation) by the Ohm's law type formulation originally proposed by van den Honert (1948)

$$\Psi_l = \Psi_s - r_{sp}\lambda E \qquad \text{(A1)}$$

E is the water flux through the soil-plant system, assumed to be equal to the total evaporation rate. The soil-plant resistance r_{sp} is considered to be the sum of a soil-root interface resistance (r_{sr}) and of a root-stem resistance (r_{rs}) assumed to be constant and equal to 0.0047 (the potentials being expressed in MPa and λE in W m^{-2}: $r_{sp} = r_{sr} + r_{rs}$. r_{sr} is given by (Lynn and Carlson, 1990; Lhomme *et al.*, 1998)

$$r_{sr} = 0.0013 k_1 / (Z_{ef} K_s) \quad \text{with} \qquad \text{(A1)}$$

$$K_s = K_{sat} (\Psi_{sat} / \Psi_s)^{3/b+2}$$

where 0.0013 (m^2) is the ratio of a parameter relating root distance and geometry to the reciprocal of the effective

rooting depth; k_1 is a conversion factor equal to 0.4×10^{-11} when r_{sr} is expressed in MPa $(Wm^{-2})^{-1}$; Z_{ef} is the effective rooting depth (m), assumed to be 1 m in our analysis; K_s is the soil hydraulic conductivity (m s^{-1}), linked to the soil water potential Ψ_s by an empirical relation (Campbell, 1974). K_{sat} and Ψ_{sat} are respectively the conductivity and the water potential at field saturation. The soil hydraulic parameters K_{sat}, Ψ_{sat} and b have been determined by Clapp and Hornberger (1978) for the 11 soil types of the USDA textural classification: b varies from 4.05 for sand to 11.4 for clay. The values retained in our simulations and shown in Table 1 correspond to a sandy clay loam. The bulk soil water potential Ψ_s is considered as an input to the model. Lhomme (1998) has recently given a detailed analysis of Eqns. (A1) and (A2), based upon a multi-layer approach, leading to a justification of van den Honert's equation. Taking into account Eqns. (8) and (A1), Eqn. (5) can be rewritten as

$$r_s = r_{i23}\left[1 + \left(\frac{\Psi_s - r_{sp}\lambda E}{\Psi_c}\right)^n\right] \text{ with} \qquad (A3)$$

$$r_{i23} = r_{s\min} F_1(S) F_2(T) F_3(D)$$

Consequently, the evaporation rate is the solution of the following transcendent equation obtained by combining Eqn. (A3) with Eqn. (1)

$$\lambda E\left\{\varepsilon + 1 + (r_{i23} / r_a)\left[1 + (\Psi_s / \Psi_c - r_{sp}\lambda E / \Psi_c)^n\right]\right\} = \varepsilon(R_n - G) + \rho\lambda D / r_a \qquad (A4)$$

The aerodynamic resistance r_a depends upon air temperature θ and surface temperature T_s (Eqn. (2)). θ is an output of the mixed-layer model and T_s is obtained by solving iteratively (up to a good convergence) the energy balance equation

$$T_s = \theta + r_a(R_n - G - \lambda E)/(\rho c_p) \qquad (A5)$$

where c_p is the specific heat of air at constant pressure. At each time step used to run the mixed-layer model, Eqns. (A4) and (A5) are solved simultaneously taking into account the air characteristics (θ and D) and radiation fluxes (S, R_n and G) of the previous step.

References

Betts, A.K., 1994. Relation between equilibrium evaporation and the saturation pressure budget. *Boundary-Layer Meteorol.*, **71**, 235–245.

Brutsaert, W., 1982. *Evaporation into the atmosphere.* D.Reidel Publishing Company, Dordrecht. 299 pp.

Brutsaert, W. and Sugita, M., 1992. Application of self-preservation in the diurnal evolution of the surface energy budget to determine daily evaporation. *J. Geophys. Res.*, 97, 18, 377–18, 382.

Campbell, G.S., 1974. A simple method for determining unsaturated conductivity from moisture retention data. *Soil Sci.*, **117**, 311–314.

Choudhury, B.J. and Idso, S.B., 1985. An empirical model for stomatal resistance of field-grown wheat. *Agric. For. Meteorol.*, **36**, 65–82.

Choudhury, B.J., Reginato, R.J. and Idso, S.B., 1986. An analysis of infrared temperature observations over wheat and calculation of latent heat flux. *Agric. For. Meteorol.*, **37**, 75–88.

Clapp, R.B. and Hornberger, G.M., 1978. Empirical equations for some soil hydraulic properties. *Wat. Resour. Res.*, 14, 601–604.

Crago, R.D., 1996a. Comparison of the evaporative fraction and the Priestley-Taylor α for parameterizing daytime evaporation. *Wat. Resour. Res.*, **32**, 1403–1409.

Crago, R.D., 1996b. Conservation and variability of the evaporative fraction during the daytime. *J. Hydrol.*, **180**, 173–194.

Crago, R.D. and Brutsaert, W., 1996. Daytime evaporation and the self-preservation of the evaporative fraction and the Bowen ratio. *J. Hydrol.*, **178**, 241–255.

Culf, A.D., 1992. An application of simple models to Sahelian convective boundary layer growth. *Boundary Layer Meteorol.*, **58**, 1–18.

Culf, A.D., 1994. Equilibrium evaporation beneath a growing convective boundary layer. *Boundary Layer Meteorol.*, **71**, 37–49.

De Bruin, H.A.R., 1983. A model for the Priestley-Taylor parameter α. *J. Clim. Appl. Meteorol.*, **22**, 572–580.

Deardorff, J.W., 1978. Efficient production of ground surface temperature and moisture with inclusion of a layer of vegetation. *J. Geophys. Res.*, **83**, 1889–1903.

de Ridder, K. and Schayes, G., 1997. The IAGL land surface model. *J. Appl. Meteorol.*, **36**, 167–182.

Huntingford, C. and Monteith, J.L., 1998. The behaviour of a mixed-layer model of the convective boundary layer coupled to a big leaf model of surface energy partitioning. *Boundary Layer Meteorol.*, **88**, 87–101.

Jacobs, C.M.J., 1994. *Direct Impact of Atmospheric CO_2 Enrichment on Regional Transpiration.* PhD thesis, Wageningen Agricultural University, The Netherlands.

Jarvis, P.G., 1976. The interpretation of leaf water potential and stomatal conductance found in canopies in the field. *Phil. Trans. R. Soc. London*, Ser. B, **273**, 593–610.

Kelliher, F.M., Leuning, R., Raupach, M.R. and Shulze, E.D., 1995. Maximum conductances for evaporation from global vegetation types. *Agric. For. Meteorol.*, **73**, 1–16.

Kim, C.P. and Entekhabi, D., 1997. Examination of two methods for estimating regional evaporation using a coupled mixed layer and land surface model. *Wat. Resour. Res.*, **33**, 2109–2116.

Kustas, W.P., Schmugge, T.J., Humes, K.S., Jackson, T.J., Parry, R., Weltz, M.A. and Moran, M.S., 1993. Relationships between evaporative fraction and remotely sensed vegetation index and microwave brightness temperature for semiarid rangelands. *J. Appl. Meteorol.*, **32**, 1781–1790.

Lhomme, J.P., 1997. An examination of the Priestley-Taylor equation using a convective boundary layer model. *Wat. Resour. Res.*, 33, 2571–2578.

Lhomme, J.P., 1998. Formulation of root water uptake in a multi-layer soil plant model: does van den Honert's equation hold? *Hydrol. Earth System Sciences*, **2**, 31–40.

Lhomme, J.P., Elguero, E., Chehbouni, A. and Boulet, G., 1998. The stomatal control of transpiration: examination of Monteith's formulation of canopy resistance. *Wat. Resour. Res.*, **34**, 2301–2308.

Lynn, B.H. and Carlson, T.N., 1990. A stomatal resistance model illustrating plant vs. external control of transpiration. *Agric. For. Meteorol.*, **52**, 5–43.

McNaughton, K.G., 1989. Regional interactions between canopies and the atmosphere. In: G. Russel et al. (Editors) *Plant Canopies: their Growth, Form and Function*, SEB seminar series, 31, Cambridge University Press.

McNaughton, K.G. and Spriggs, T.W., 1986. A mixed-layer model for regional evaporation. *Boundary-Layer Meteorol.*, **34**, 243–262.

McNaughton, K.G. and Spriggs, T.W., 1989. An evaluation of the Priestley-Taylor equation and the complementary relationship using results from a mixed-layer model of the convective boundary layer. In: *Estimation of Areal Evapotranspiration*, IAHS Publ. **177**, 89–104.

Mascart, P., Taconet, O., Pinty, J.P. and Ben Mehrez, M., 1991. Canopy resistance formulation and its effect in mesoscale models: a HAPEX perspective. *Agric. For. Meteorol.*, **54**, 319–351.

Monteith, J.L., 1981. Evaporation and surface temperature. *Quart. J. R. Meteorol. Soc.*, **107**, 1–27.

Monteith, J.L., 1995. Accomodation between transpiring vegetation and the convective boundary layer. *J. Hydrol.*, **166**, 251–263.

Nichols, W.E. and Cuenca, R.H., 1993. Evaluation of the evaporative fraction for parameterization of the surface energy balance. *Wat. Resour. Res.*, **29**, 3681–3690.

Noilhan, J. and Planton, S., 1989. A simple parameterization of land surface processes for meteorological models. *Monthly Weather Rev.*, **117**, 536–549.

Raupach, M.R., 1998. Influences of local feedbacks on land-air exchanges of energy and carbon. *Global Change Biology*, **4**, 477–494.

Raupach, M.R., Denmead, O.T. and Dunin, F.X., 1992. Challenges in linking atmospheric CO_2 concentrations to fluxes at local and regional scales. *Aust. J. Bot.*, **40**, 697–716.

Shuttleworth, W.J., Gurney, R.J., Hsu, A.Y. and Ormsby, J.P., 1989. FIFE: the variation in energy partition at surface flux sites. In: *Proceedings of the IAHS Third International Assembly*, IAHS Publ. **186**, 67–74.

Stewart, J.B., 1988. Modelling surface conductance of pine forest. *Agric. For. Meteorol.*, **43**, 19–37.

Stewart, J.B., 1996. Extrapolation of evaporation at time of satellite overpass to daily totals. In: J.B. Stewart *et al.* (editors) *Scaling up in Hydrology using Remote Sensing*. Wiley, Chichester, UK.

Stewart, J.B. and Gay, L.W., 1989. Preliminary modelling of transpiration from the FIFE site in Kansas. *Agric. For. Meteorol.*, **48**, 305–315.

Sugita, M. and Brutsaert, W., 1991. Daily evaporation over a region from lower boundary layer profiles measured with radiosondes. *Wat. Resour. Res.*, **27**, 747–752.

van den Honert, T.H., 1948. Water transport in plants as a catenary process. *Discuss. Faraday Soc.*, **3**, 146–153.